Taylor & Francis
Taylor & Francis Group

Combustion Science and Technology

ISSN: 0010-2202 (Print) 1563-521X (Online) Journal homepage: https://www.tandfonline.com/loi/gcst20

The Physics of Scalar Gradients in Turbulent Premixed Combustion and Its Relevance to Modeling

Cesar Dopazo & Luis Cifuentes

To cite this article: Cesar Dopazo & Luis Cifuentes (2016) The Physics of Scalar Gradients in Turbulent Premixed Combustion and Its Relevance to Modeling, Combustion Science and Technology, 188:9, 1376-1397, DOI: 10.1080/00102202.2016.1197919

To link to this article: https://doi.org/10.1080/00102202.2016.1197919

COMBUSTION SCIENCE AND TECHNOLOGY
2016, VOL. 188, NO. 9, 1376–1397
http://dx.doi.org/10.1080/00102202.2016.1197919

Taylor & Francis
Taylor & Francis Group

The Physics of Scalar Gradients in Turbulent Premixed Combustion and Its Relevance to Modeling

Cesar Dopazo and Luis Cifuentes

School of Engineering and Architecture, Fluid Mechanics Area, University of Zaragoza, Zaragoza, Spain

ABSTRACT

Equations for the absolute value of the scalar gradient and for the infinitesimal distance, Δx_N, between two adjacent iso-scalar non-material surfaces are obtained. 'Effective' strain rate normal to the iso-surfaces, which includes flow and physicochemically 'added' contributions, is shown to be an essential variable, causing either enhancement or destruction of scalar gradients and reduction or growth of distances between surfaces. Two DNS datasets for turbulent premixed flames, one simulating a statistically planar propagating front in an inflow-outflow configuration and the other computing a jet of a methane-air mixture, surrounded by a coflow of hot products, have been examined. DNS are used to estimate the relative importance of different processes determining the gradients fate. The flow normal strain rate apparently scales with the inverse of the Kolmogorov time microscale. Using as characteristic time, δ_L/S_L, and length, δ_L, where δ_L and S_L are the laminar flame thickness and propagating velocity, a dimensionless equation for the time rate of change of $\Delta x_N/\delta_L$ depends on five dimensionless parameters, among them the Karlovitz number, Ka; the contribution of every term in the rate equation depends on the magnitude of Ka compared to the other dimensionless groups. The chemically 'added' normal strain rate dominates the time evolution of $\Delta x_N/\delta_L$ in the burning and a good share of the preheat regions of the statistically planar flame, whereas 'added' and flow normal strain rates are comparable in the turbulent jet flame. Large values of some of these dimensionless parameters hint at the likely importance of accounting for Reynolds and/or Damhöhler numbers dependencies in future work. A consistent definition of an average premixed turbulent flame thickness is presented and its computed values are compared to a previous proposal. Some suggestions to model the molecular mixing term in the context of the scalar PDF transport methodology are discussed. It is hypothesized that the characteristic mixing time should be proportional to the inverse of the 'effective' normal strain rate.

ARTICLE HISTORY
Received 15 October 2015
Revised 6 May 2016
Accepted 25 May 2016

KEYWORDS
Flow, 'added' and 'effective' normal strain rates; Iso-scalar non-material surfaces; Karlovitz number; Molecular mixing models; Probability density function transport; Scalar gradients; Turbulent flame mean thickness

1. Introduction

Premixed combustion is currently of interest, among other things, because it is essential in the development of low NOx emission gas turbines. Premixed (Swaminathan and Bray, 2011) and partially premixed (Masri, 2015) systems are receiving much attention. Molecular mixing and chemical conversion are strongly coupled for every participating

CONTACT Luis Cifuentes luis.cifuentes@mech.kth.se Royal Institute of Technology—Linné FLOW Centre, KTH Mechanics, Osquars Backe 18, Stockholm 10044, Sweden.

Color versions of one or more of the figures in the article can be found online at www.tandfonline.com/gcst.

scalar (e.g., reaction progress variable or/and temperature). Molecular diffusive fluxes depend on scalar gradients, which evolve in response to the turbulence/chemistry interactions.

Chakraborty and Cant (2004) obtained from DNS two closely related quantities: the gradient magnitude of the reaction progress variable and the displacement speed of every iso-surface; they examined the unsteady effects of tangential strain rates and curvatures upon flame propagation. Chakraborty and Cant (2005) also found that for different Lewis numbers both dilatation and tangential strain rate are negatively correlated with curvature.

Swaminathan and Grout (2006) analyzed turbulent premixed flame DNS datasets and clearly identified differences between "scalar gradient production by incompressible turbulence, via their preferential alignment with the most compressive principal strain rate" (Ashurst et al., 1987), and destruction, due to their predominant "alignment with the most extensive principal strain rate," for a turbulent premixed flame, "having flamelet combustion characteristics." The authors argue that flow dilatation pulls the iso-scalar surfaces from each other, dissipating scalar gradients in premixed flames when the Damköhler number is large; this process is counteracted by chemical reactions, which produce scalar gradients.

Chakraborty (2007) showed that the gradient modulus of the reaction progress variable is governed by the volumetric dilatation rate in a high Damköhler number flame, while it is affected by the flow tangential strain rate in the low Damköhler number case; the flow normal strain rate was positive across the flame brush in the former case, whereas it was negative in the latter. He concluded that the relative strength of the dilatation rate and the tangential strain rate on a given iso-surface determined the behavior of scalar gradients. However, the essential role of the normal strain rates on the gradient fate was not explicitly identified.

Chakraborty and Swaminathan (2007) found that "the well known alignment of scalar gradient with the most compressive principal strain rate resulting in production of the scalar gradient by turbulence is observed for a low Damköhler (Da) number flame, whereas the turbulence dissipates the scalar gradient in high Da flame." The preferential alignment of the scalar gradient with the most extensive principal strain rate was considered the reason for its dissipation in the high Da flame. In regions of intense heat release, the scalar gradient tends to align with the most extensive strain rate, even for $Da < 1$. It was argued that scalar gradient destruction is due to a strong competition between chemical strain rate, "due to dilatation from the flame front" and the local flow strain rate. The authors obtained positive flame normal strain rates throughout the flame brush when $Da > 1$, whereas negative values predominate when $Da < 1$.

Chakraborty, Klein, and Swaminathan (2009) investigated Lewis (Le) number effects on reactive scalar gradient alignments with local strain rates using DNS data of freely propagating statistically planar turbulent premixed flames. The alignment characteristics are explained using the statistics of dilatation rate, and flame normal and tangential strain rates; dilatation rates increase as Le decreases, particularly for $Le < 1$; reactive scalar gradients align with the most extensive principal strain rate in the reaction zone for flames with Le around unity. However, in flames with $Le < 1$ the scalar gradient is parallel to the eigenvector of the most extensive principal strain rate for most of the flame brush.

Hartung et al. (2008) used stereoscopic PIV and PLIF to investigate premixed ethylene-air flames stabilized on a bluff body. They examined the alignment of the flame normal

unit vector and the strain rate eigenvectors and found that the most extensive strain rate aligns with the normal. The flow normal strain rate is positive, which implies that scalar gradients are destroyed by the turbulent flow "as the scalar iso-surfaces are pulled apart." The authors argued that "this questions the validity of passive scalar turbulence physics commonly used for premixed flame modeling." Steinberg et al. (2012) applied stereoscopic PIV to turbulent premixed Bunsen flames. The most extensive principal strain rate associated with the turbulence is preferentially aligned with the flame surface normal direction.

Sankaran et al. (2007) analyzed DNS results of a 3D spatially developing turbulent slot-burner Bunsen premixed flame with a reduced methane-air mechanism. The combustion occurs in the thin reaction zones regime. The mean thickness of the turbulent flame is defined in terms of the modulus of the reaction progress variable gradient; the influences of the tangential strain rate and the flame front curvature on that mean flame thickness are examined. A transport equation for the modulus of the gradient of the reaction progress variable is presented and flow strain rates and some components of the derivative of the propagation speed normal to the flame front are obtained, conditional upon the curvature.

Aris (1962) obtained expressions for the strain and stress in a material surface, as well as intrinsic equations for the surface motion. Pope (1988) stated that turbulent mixing "can be described to advantage in terms of surfaces" and investigated theoretically the evolution of material, propagating, and constant-property surfaces in a turbulent flow through the use of intrinsic coordinates; the stretch factors for a surface element area are expressed in terms of the flow tangential strain rate and the curvature effect on a propagating interface. He also presents a probabilistic description of the expected surface-to-volume ratio.

Cifuentes (2015) and Dopazo et al. (2015a, 2015b) derived equations for the unitary rate of change of: (i) an infinitesimal area element on a non-material iso-scalar surface, (ii) the normal distance between two neighboring surfaces, and (iii) an elementary volume formed by the two previous geometric objects. They used classical and simple tools to analyze fluid motion in the neighborhood of a point. A transport equation for the absolute value of the scalar gradient was derived, similar to that previously proposed by Sankaran et al. (2007). Molecular diffusion and chemical reaction processes induce strain rates in the tangential and normal directions to a scalar iso-surface, which produce additional deformation to those caused by the flow strain rates. This description provides a simple framework to explain either enhancement or destruction of scalar gradients. Scalar gradient behavior in constant density turbulent mixing and reaction systems, as well as in premixed flames, were studied using existing DNS databases (Dopazo et al., 2015b). The effect of flow strain rates plus the added ones, due to diffusion and reaction, on scalar gradients and very likely on mixing, are significantly different without and with volumetric dilatation rates, which are typical of combusting flows.

Swaminathan and Bray (2011) discuss different modeling strategies for turbulent premixed flame prediction, including closures of the turbulent transport and of the reaction rate, for both RANS and LES. It is well known that chemical conversion terms can be advantageously treated with the PDF transport methodology, wherein only molecular mixing contributions must be modeled (Celis and Da Silva, 2015; Dopazo, 1994; Dopazo and O'Brien, 1974; Haworth, 2010; O'Brien, 1980); the latter are related to the evolution of scalar gradients and their derivatives on iso-surfaces. Monte Carlo methods,

needed to solve PDF transport equations (Flagan and Appleton, 1974; Pope, 1985), can be applied to simulate models involving scalar gradients and scalar second derivative normal to iso-surfaces (Dopazo et al., 2015b). The surface density function methodology (Vervisch et al., 1995) is also closely related to the scalar gradient modulus.

The main objectives of the present work are:

(1) to estimate the orders of magnitude of the various contributions to the added normal strain rate, due to diffusion and reaction, compared with the flow normal strain rate;
(2) to introduce a new definition of a turbulent flame thickness, based on the infinitesimal distance between two adjacent iso-scalar surfaces; and
(3) to further explore the conjecture that the unitary time rate of change of the infinitesimal distance between neighboring iso-surfaces provides a meaningful characteristic mixing time to be used in PDF molecular mixing models.

To meet these objectives, DNS datasets for two premixed combustion configurations are examined.

Section 2 summarizes the mathematical background proposed to explain the DNS data, which are briefly described in Section 3. Results are presented in Section 4, with some discussions and new proposals. Section 5 presents some modeling reflections, which are restricted to the molecular mixing term in the context of scalar PDF transport methodologies. Some conclusions are drawn in Section 6, and needs of further work are outlined.

2. Theoretical background

Space and time evolution of iso-scalar surfaces provide a physically sound explanation for mixing and reacting systems. The reduced mass fraction (defined differently for the two DNS datasets in Section 3), $Y(\mathbf{x},t)$, characterizes the iso-surface, $Y(\mathbf{x},t)=\Gamma$. Y is unity in the fresh reactants and vanishes in the hot products (see Figure 1). A point, $\mathbf{x}$, on that surface moves with a speed, $\mathbf{v}^Y(\mathbf{x},t)$, at time t, given by:

$$\mathbf{v}^Y(\mathbf{x},t)=\mathbf{v}(\mathbf{x},t)+V(\mathbf{x},t)\mathbf{n} \tag{1}$$

where $\mathbf{v}(\mathbf{x},t)$ is the local and instantaneous flow velocity, and $V(\mathbf{x},t)$ is the iso-surface propagating speed, relative to the fluid in its normal direction, $\mathbf{n}(\mathbf{x},t)$, which is defined by:

$$n_i(\mathbf{x},t)=\frac{1}{|\nabla Y|}\frac{\partial Y}{\partial x_i} \tag{2}$$

The absolute value of the scalar gradient is expressed as:

$$|\nabla Y|=\frac{\partial Y}{\partial x_N} \tag{3}$$

where x_N is the local coordinate, normal to the iso-surface, and positive in the direction of $\mathbf{n}$.

The non-material surface $Y(\mathbf{x},t)=\Gamma$ obeys the kinematic equation:

$$\frac{\partial Y}{\partial t}+v_j^Y\frac{\partial Y}{\partial x_j}=0 \tag{4}$$

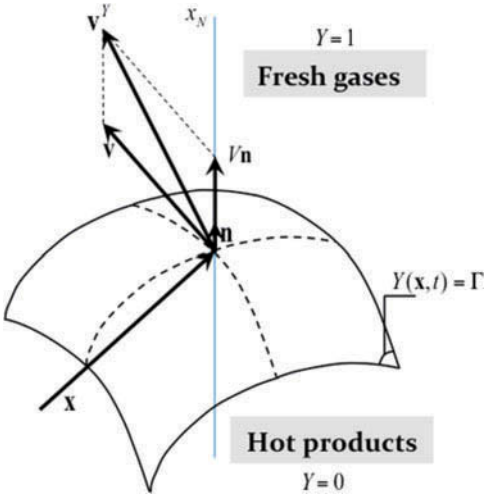

Figure 1. Iso-scalar surface $Y(\mathbf{x},t)=\Gamma$, velocities of a point $\mathbf{x}$ at time t and unit normal vector, $\mathbf{n}(\mathbf{x},t)$.

which might be rephrased as:

$$\frac{\partial Y}{\partial t}+v_j\frac{\partial Y}{\partial x_j}=-V|\nabla Y| \tag{5}$$

The conservation equation for $Y(\mathbf{x},t)$ is:

$$\frac{\partial Y}{\partial t}+v_j\frac{\partial Y}{\partial x_j}=\frac{1}{\rho}\frac{\partial}{\partial x_j}\left(\rho D\frac{\partial Y}{\partial x_j}\right)+\frac{\dot{\omega}}{\rho} \tag{6}$$

where ρ is the fluid density, D is the molecular diffusion coefficient, and $\dot{\omega}$ is the chemical reaction rate. The diffusion term can be expressed in terms of normal derivatives, yielding for Eq. (6) (Cifuentes, 2015; Dopazo et al., 2015a, 2015b; Echekki and Chen, 1999):

$$\frac{\partial Y}{\partial t}+v_j\frac{\partial Y}{\partial x_j}=D\left(\frac{1}{\rho D}\frac{\partial \rho D}{\partial x_N}\right)\frac{\partial Y}{\partial x_N}+D\frac{\partial^2 Y}{\partial x_N^2}+2k_mD\frac{\partial Y}{\partial x_N}+\frac{\dot{\omega}}{\rho} \tag{7}$$

Equating the right sides of Eqs. (5) and (7), $V(\mathbf{x},t)$ is expressed as:

$$V(\mathbf{x},t)=-D\left(\frac{1}{\rho D}\frac{\partial \rho D}{\partial x_N}\right)-D\frac{\partial^2 Y/\partial x_N^2}{(\partial Y/\partial x_N)}-2k_mD-\frac{\dot{\omega}}{\rho(\partial Y/\partial x_N)} \tag{8}$$

The time rates of change of infinitesimal non-material elements, such as a vector, $\mathbf{r}=\Delta x_N\mathbf{n}$; joining points $\mathbf{x}$ and $\mathbf{x}+\mathbf{r}$ on two iso-surfaces, $Y(\mathbf{x},t)=\Gamma$ and $Y(\mathbf{x},t)=\Gamma+\Delta\Gamma$, respectively; a surface area, S; and a volume, $\vee=\mathrm{S}\Delta x_N$ (see Figure 2), are expressed as (Cifuentes, 2015; Dopazo et al., 2015a, 2015b):

$$\frac{1}{\Delta x_N}\frac{d\Delta x_N}{dt}=a_N+\frac{\partial V}{\partial x_N} \tag{9}$$

$$\frac{1}{\mathrm{S}}\frac{d\mathrm{S}}{dt}=a_T+2k_mV \tag{10}$$

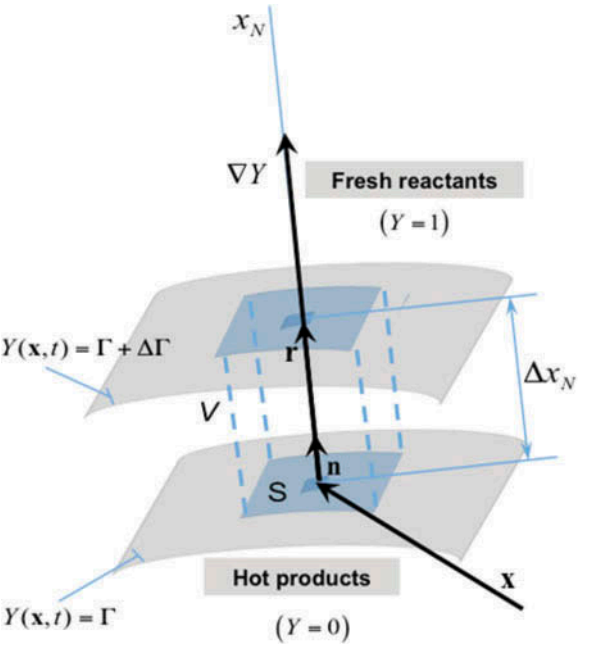

Figure 2. Two adjacent non-material iso-scalar surfaces, an infinitesimal vector, **r**, joining two points on these surfaces, an infinitesimal surface area, S, on $Y(\mathbf{x},t)=\Gamma$, and an infinitesimal volume, $\vee$.

$$\frac{1}{\vee}\frac{d\vee}{dt}=\frac{\partial v_i^Y}{\partial x_i}=a_N+\frac{\partial V}{\partial x_N}+a_T+2k_mV \tag{11}$$

where a_N and a_T are the flow strain rates, normal and tangential, respectively, to the iso-surface $Y(\mathbf{x},t)=\Gamma$, given by:

$$a_N=n_is_{ij}n_j \tag{12}$$

$$a_T=\left(\delta_{ij}-n_in_j\right)s_{ij} \tag{13}$$

The flow strain rate tensor, s_{ij}, is conventionally defined by:

$$s_{ij}=\frac{1}{2}\left(\frac{\partial \mathrm{v}_i}{\partial x_j}+\frac{\partial \mathrm{v}_j}{\partial x_i}\right) \tag{14}$$

$k_m=0.5\partial n_i/\partial x_i$ is the mean curvature of the iso-surface at point **x** and time t. Note that the flow volumetric dilatation rate, $\partial v_i/\partial x_i$, is:

$$\frac{\partial v_i}{\partial x_i}=a_N+a_T \tag{15}$$

An expression for $\partial V/\partial x_N$, which appears in Eqs. (9) and (11), is formally derived from Eq. (8), namely:

$$\frac{\partial V}{\partial x_N}=\underbrace{\frac{\partial}{\partial x_N}\left[-D\left(\frac{1}{\rho D}\frac{\partial \rho D}{\partial x_N}\right)\right]}_{(\partial V/\partial x_N)_1}+\underbrace{\frac{\partial}{\partial x_N}\left[-D\frac{\partial^2 Y/\partial x_N^2}{(\partial Y/\partial x_N)}\right]}_{(\partial V/\partial x_N)_2}+\underbrace{\frac{\partial}{\partial x_N}(-2k_mD)}_{(\partial V/\partial x_N)_3}+\underbrace{\frac{\partial}{\partial x_N}\left[-\frac{\dot{\omega}}{\rho(\partial Y/\partial x_N)}\right]}_{(\partial V/\partial x_N)_4} \tag{16}$$

The various 'added' strain rates are: $(\partial V/\partial x_N)_1$, due to ρD variations normal to the iso-surface; $(\partial V/\partial x_N)_2$, caused by the normal molecular diffusion; $(\partial V/\partial x_N)_3$, the effect of tangential diffusion (curvature); and $(\partial V/\partial x_N)_4$, induced by the chemical reaction. The first and second terms can also be treated jointly (Echekki and Chen, 1999).

The right sides of Eqs. (9) and (10) contain the additive contributions of the flow, a_N, and 'added', $\partial V/\partial x_N$, normal strain rates, as well as the flow, a_T, and the 'added', $2k_m V$, tangential strain rates. The 'added' strain rates are due to the non-material nature of the iso-surfaces, the normal one because of the different velocities of two adjacent surfaces and the tangential one as a result of the propagation relative to the fluid of curved fronts. The addition of flow and 'added' strain rates can be termed 'effective' strain rates.

The modulus of the scalar gradient in terms of infinitesimal increments is given by:

$$|\nabla Y| \approx \frac{\Delta\Gamma}{\Delta x_N} \tag{17}$$

The scalar dissipation rate adopts the expression:

$$\varepsilon_Y = D\left(\frac{\partial Y}{\partial x_N}\right)^2 \approx D\left(\frac{\Delta\Gamma}{\Delta x_N}\right)^2 \tag{18}$$

An evolution equation for $|\nabla Y|$ can be easily derived from Eq. (4):

$$\frac{\partial|\nabla Y|}{\partial t} + v_j^Y \frac{\partial|\nabla Y|}{\partial x_j} = -\left(a_N + \frac{\partial V}{\partial x_N}\right)|\nabla Y| \tag{19}$$

Equation (19) is the correct version of Eq. (2) of Sankaran et al. (2007), wherein the left-hand side was replaced by the material derivative. Equation (9) can be expanded to read:

$$\begin{aligned}\frac{1}{\Delta x_N}\frac{d\Delta x_N}{dt} = a_N &+ \frac{\partial}{\partial x_N}\left[-D\left(\frac{1}{\rho D}\frac{\partial \rho D}{\partial x_N}\right)\right] + \frac{\partial}{\partial x_N}\left[-D\frac{\partial^2 Y/\partial x_N^2}{(\partial Y/\partial x_N)}\right] \\ &+ \frac{\partial}{\partial x_N}(-2k_m D) + \frac{\partial}{\partial x_N}\left[-\frac{\dot{\omega}}{\rho(\partial Y/\partial x_N)}\right]\end{aligned} \tag{20}$$

Every term in Eq. (20) has dimensions of the inverse of a time. a_N, the flow normal strain rate, is very likely proportional to the inverse of the Kolmogorov time microscale, $\tau_\eta = (\nu/\varepsilon)^{1/2}$. Yeung et al. (1990) obtained, from a DNS of constant-density, statistically stationary, homogeneous, and isotropic turbulence undergoing forcing of the velocity field, that a_T, acting on thin diffusive layers, is approximately equal to τ_η^{-1}. The time arising from the variations of ρD normal to the iso-surface is written as:

$$\tau_{\rho D} = \frac{1}{\frac{\partial}{\partial x_N}\left[-D\left(\frac{1}{\rho D}\frac{\partial \rho D}{\partial x_N}\right)\right]} \tag{21}$$

The time induced by the normal molecular diffusion is defined by:

$$\tau_{ND} = \frac{1}{\frac{\partial}{\partial x_N}\left[-D\frac{\left(\partial^2 Y/\partial x_N^2\right)}{(\partial Y/\partial x_N)}\right]} \tag{22}$$

while that resulting from the tangential diffusion is given by:

$$\tau_{curv} = \frac{1}{\frac{\partial}{\partial x_N}\left[-D2k_m\right]} \tag{23}$$

The time associated to the chemical conversion term is:

$$\tau_{chem} = \frac{1}{\frac{\partial}{\partial x_N}\left[-\frac{\dot{\omega}}{\rho(\partial Y/\partial x_N)}\right]} \tag{24}$$

Alternatively, some contributions to the right side of (20) can better be rephrased in terms of length variables, namely, $\delta_{\rho D} = \left(D\tau_{\rho D}\right)^{1/2}$, $\delta_{ND} = \left(D\tau_{ND}\right)^{1/2}$, and $\delta_{curv} = \left(D\tau_{curv}\right)^{1/2}$. The latter will include normal derivatives of the mean curvature. Time variables (21)–(24) and the corresponding lengths, $\delta_{\rho D}$, δ_{ND}, and δ_{curv}, will be obtained from the DNS datasets.

3. DNS datasets examined

Two DNS datasets of turbulent premixed flames have been examined and compared in this work:

- A propagating premixed turbulent statistically planar flame in an inflow-outflow configuration with a single step Arrhenius-type irreversible chemical reaction (see Figure 3)
- A turbulent jet premixed flame in a coflow of hot products with detailed methane-air chemistry (see Figure 4)

Numerical values of the aero-thermochemical variables for the two simulations are presented in Table 1.

3.1. *Turbulent premixed flame in an inflow-outflow configuration*

Initial conditions correspond to a planar premixed flame propagating in the negative x direction with the laminar flame speed, S_L, towards the fresh gases. The flame encounters a decaying turbulent field, which wrinkles it as it progresses. The initial constant-density isotropic turbulence is generated with an independent pseudo-spectral numerical code (Orszag and Patterson, 1972), starting from a given spectrum and using a stochastic forcing to yield a statistically stationary field. Conservation equations of mass, momentum, energy, and chemical species are solved using the fully parallel compressible solver NTMIX3D (Cuenot et al., 1997). The full set of governing equations is made dimensionless using as reference characteristic variables and molecular transport coefficients in the fresh gases the speed of sound, a_{ref}, the density and temperature and a characteristic length, L_{ref}, defined as $L_{ref} = \left(Re_{ac}\nu_{ref}\right)/a_{ref}$; ν_{ref} is the kinematic viscosity and $Re_{ac}(= 5000)$ is a scaling parameter. The rms velocity fluctuations in the 'fresh reactants' decay from $u_0^{'} = 0.016$ at $t = 0$ to $u' = 0.01$ at t_{final}, in which our data are obtained. To estimate the integral length scale, l, in the 'fresh reactants', the transverse autocorrelation coefficients in cross-stream planes, $y - z$, are computed. The integral scale increases from $l_0 = 1.058$ at $t = 0$ to $l = 1.20$ at t_{final}. The turbulent Reynolds number, $Re = u'l/\nu$,

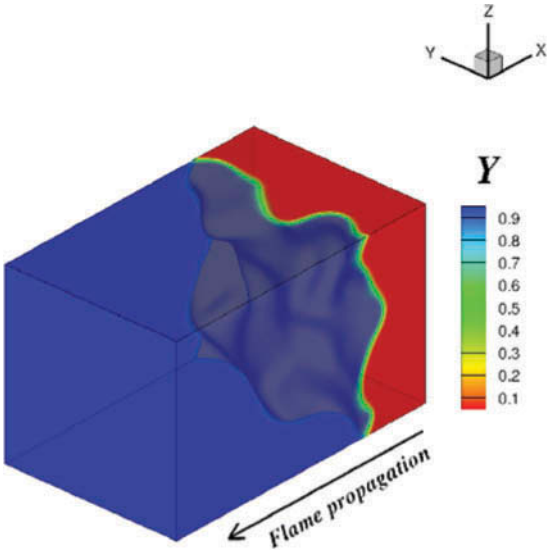

Figure 3. Computational domain for the DNS of a turbulent premixed flame in an inflow-outflow configuration.

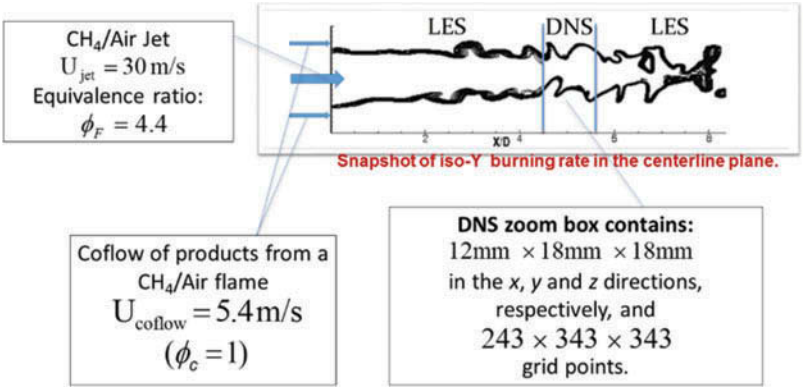

Figure 4. Computational domain for the DNS of a turbulent jet premixed flame in a coflow.

decreases from $Re = 86$ at $t = 0$ to $Re = 61$at t_{final}. The initial eddy turnover time is $\tau_0 = l_0/u_0^{'} = 66.13$. In this study, the initially planar laminar flame is allowed to interact with the turbulence field up to a time $t_{final} = 90$, whichis1.36 times greater than the initial eddy turnover time. The domain is considered periodic in the y and z directions, while non-reflecting inlet-outlet boundary conditions are imposed in the x direction, using the Navier–Stokes characteristic boundary condition (NSCBC) method (Poinsot and Lele, 1992). The solver uses a sixth-order compact finite-difference scheme for space discretization, and a third-order Runge–Kutta explicit method for time integration. The computational domain, shown schematically in Figure 3, has a size 3π in the x direction and 2π in

Table 1. DNS dimensional variables and dimensionless parameters.

	Configuration	
Variables and dimensionless parameters	Inflow-outflow	Jet in co-flow
Integral length scale, l	1.20	2.4 (mm)
Velocity fluctuations rms, u'	0.01	2.12 (m/s)
Kinematic viscosity, ν	1.9739×10^{-4}	$1.7 \times 10^{-5}(\mathrm{m}^2/\mathrm{s})$
Turbulent kinetic energy dissipation rate, $\varepsilon = u'^3/l$	8.333×10^{-7}	$4.0 \times 10^{3}(\mathrm{m}^2/\mathrm{s}^3)$
Kolmogorov length micro-scale, $\eta = (\nu^3/\varepsilon)^{1/4}$	0.055	0.0332 (mm)
Kolmogorov time micro-scale, $\tau_\eta = (\nu/\varepsilon)^{1/2}$	15.4	0.0651 (ms)
Non-stretched laminar flame speed, S_L	0.005	0.39 (m/s)
Laminar flame thickness, δ_L	0.0526	0.38 (mm)
Final velocity ratio, u'/S_L	2.0	5.43
Chemical time scale, $\tau_{ch} = \delta_L/S_L$	10.40	0.9743 (ms)
Final length ratio, l/δ_L	22.81	6.31
Turbulent Reynolds number, Re	61	300
Karlovitz number, Ka	0.675	14.96
Zeldovich number, β	6.0	—
Prandtl number, Pr	0.75	0.72
Schmidt number, Sc	0.75	0.72
Lewis number, Le	1.0	1.0

the y and z directions, and contains $768 \times 512 \times 512$ grid points, uniformly distributed. The reaction rate expression used is:

$$\dot{\omega} = \rho Y B_0 \exp(-\beta/\alpha) \exp[-\beta Y/(1-\alpha Y)] \tag{25}$$

where ρ is the fluid density, $Y = Y_R/Y_R^u$ is the reduced mass fraction of the mixture (Y_R is the reactants mass fraction and Y_R^u denotes its value in the fresh gases), B_0 is the pre-exponential factor, $\alpha = (T_b - T_u)/T_b$ is the temperature ratio defined with the local temperature, T, that in the unburned reactants, T_u, and that in the burned products, T_b, β, is the reduced activation energy or Zel'dovich number, $\beta = \alpha E_a/RT_b$, E is the activation energy, and R is the perfect gas constant. The fluid obeys the perfect gas equation of state, with constant molecular mass and constant specific heat ratio γ. The dynamic viscosity is temperature dependent, $\mu = \mu_u(T/T_u)^b$, with $b = 0.6$. The Schmidt, $Sc = 0.75$, and Prandtl, $Pr = 0.75$, numbers are constant and the chemical rate parameters are $\alpha = 0.8$ and $\beta = 6.0$. The mass diffusivity D and the thermal diffusivity D_{th} are given by $D = \mu/\rho Sc$ and $D_{th} = \mu/\rho Pr$. The flame thickness is defined as $\delta_L = D_{th}/S_L = 0.0526$. The Karlovitz number, defined as $Ka = \tau_{ch}/\tau_\eta$, is 0.67 at t_{final}. Therefore, combustion takes place in the "corrugated flamelets" regime (Borghi, 1985; Poinsot and Veynante, 2005).

3.2. *Turbulent jet premixed flame in a coflow*

The second dataset analyzed is a hybrid LES–DNS of a stoichiometric methane-air mixture, which is injected through a central jet with a mean velocity of $U_{jet} = 30\mathrm{m/s}$ and an equivalence ratio of $\emptyset_F = 4.4$, surrounded by a coflow of burned products with a mean velocity of $U_{cofl} = 5.4\mathrm{m/s}$ and equivalence ratio of $\emptyset_c = 1$. The nozzle diameter is $D = 12\mathrm{mm}$ and the computational domain extends 192 mm in the streamwise (x), 66 mm in the crosswise (y), and 66 mm in the spanwise (z) directions, with 802, 466, and 466 grid points, uniformly spaced, in the x, y, and z directions, respectively (see Figure 4). This LES-DNS-LES dataset has been previously used and checked (Cifuentes et al., 2014, 2016).

The strategy is to perform an imbedded DNS, which is forced at its inlet by well-refined LES results provided by the solution of the slightly filtered Navier–Stokes equations upstream of the DNS zone. Questions might arise on the LES requirements to resolve a maximum share of kinetic energy and scalar variance, as well as on the modeled velocity and scalar fluctuation dissipation rates and their correlation. Nevertheless, should the numerical scheme be non-dissipative, sufficient refinement of the grid starting from one, which already captures most of the flow structures, leads to a very rapid development within a small downstream distance of the smallest scales, and DNS resolution is reached. The latter is certainly relevant to micro-mixing and combustion. The LES mesh has about 171 million nodes, with grid sizes varying between 150 and 200 micrometers. An imbedded zone within the LES mesh features a higher resolution. Results are analyzed in this DNS zoom box located at the jet centerline at $x/D = 4.5$ from the nozzle, and at $t = 80$ms, which is much greater than the initial integral eddy turnover time, $\tau_0 = 1.13$ms. The DNS zoom box contains $243 \times 343 \times 343$ points with grid sizes of the order of 50 micrometers in the x, y, and z directions, which ensures more than 70 grid points within the flame thickness, $\delta_L = (T_b - T_u)/\max(|\nabla T|) = 0.38$mm, and more than 6 within the Kolmogorov length microscale. Subscripts u and b indicate variables in the unburned and burned gases, respectively, and T is the local temperature field. The convective terms have been computed with a fourth-order centered skew-symmetric-like scheme, and the diffusive terms with a fourth-order centered scheme. The time integration used a third-order Runge–Kutta scheme. All boundary conditions are imposed using the 3D-NSCBC approach (Poinsot and Lele, 1992).

Pre-computed look-up tables for evaluating the chemical kinetics are utilized. A reduced mass fraction, $Y = 1 - \left(Y_c/Y_c^{eq}\right)$, based on a single progress variable, $Y_c = Y_{CO} + Y_{CO_2} + \left(Y_{N_2} + Y_{N_2}^0\right) + \left(Y_{H_2O} + Y_{H_2O}^0\right) + Y_{NO} + Y_{N_2O}$, is used, where the '*eq*' superscript designates the value of the corresponding variable in the burned state of the laminar-premixed flame. $Y_{N_2}^0$ and $Y_{H_2O}^0$ are, respectively, the mass fractions of N_2 and H_2O in the fresh gases, which ensure that $Y_c = 0$ in the unreacted region for all mixing conditions. This simulation was performed with the fully parallel compressible solver SiTCom (simulating turbulent combustion) (Cifuentes et al., 2014, 2016), which integrates the mass, momentum, energy, and reaction progress variable conservation equations. Thermodynamic variables are related through the perfect gas law. Viscosity, thermal conductivity, and mass diffusion coefficients are given functions of the temperature. The Karlovitz number is $Ka = \tau_{ch}/\tau_\eta = 14.96$ with combustion taking place in the 'thickened-wrinkled flame' regime (Borghi, 1985; Poinsot and Veynante, 2005).

4. Results and discussion

Figure 5 depicts the average chemical reaction rate conditional upon Y for the two flames. Vertical dashed lines delimit the different flame regions: fresh reactants ($0.70 < Y < 1.00$), preheat ($0.35 < Y \leq 0.70$), and burning ($0.05 < Y \leq 0.35$ for the statistically planar flame, $0.15 < Y \leq 0.35$ for the jet flame) zones, and hot products ($Y \leq 0.05$ for the statistically planar flame, $Y \leq 0.15$ for the jet flame) (Cifuentes, 2015; Dopazo et al., 2015a). The different limits between hot-product and burning regions for the statistically planar and the jet configurations are due to the coflow of hot products in the jet flame, which modifies

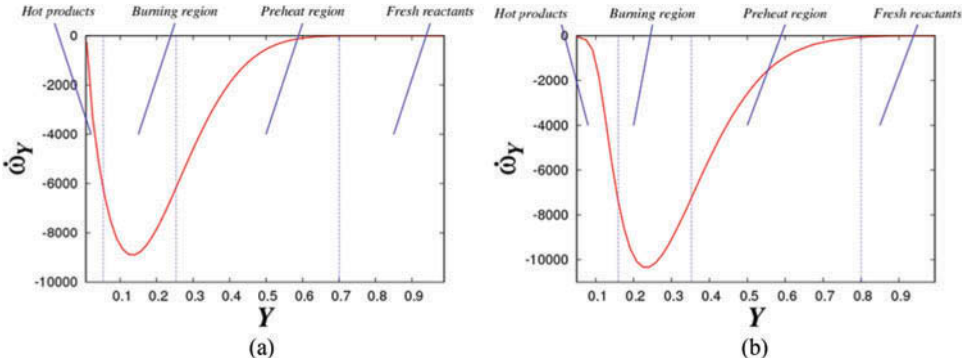

Figure 5. Average reaction rate, $\dot{\omega}_Y = \dot{\omega}/\rho$, conditional upon the value of Y for (a) statistically planar turbulent premixed flame and (b) turbulent jet premixed flame in a coflow.

the value of the reaction rate. These limits among the various flame regions are merely indicative.

The terms on the right side of Eq. (16) are plotted in Figure 6 for the two DNS datasets examined. The average flow normal strain, a_N, is apparently negligible compared to the 'added' normal strain, $\partial V/\partial x_N$, in the highly reactive region $(0.35 < Y < 0.05)$ of the statistically planar flame; whereas the average a_N is predominantly positive, $\partial V/\partial x_N$ is mostly negative. The reduction of Δx_N and, thus, the scalar-gradient growth are mainly due to a balance between destruction by normal diffusion and enhancement by chemical reaction, although the chemical strain is almost four times greater than the normal diffusion one. The flow strain and the 'added' strain by ρD variations tend to become comparable to the normal diffusion and chemical contributions for $Y > 0.45$, in a part of the preheat zone $(0.35 < Y < 0.70)$. Average mean curvature effects are negligible over most of the computational domain. On the other hand, for the jet flame configuration a_N and $\partial V/\partial x_N$ are of the same order in both the preheat and the burning regions; the important contributions to $\partial V/\partial x_N$ in the burning zone come from chemistry and

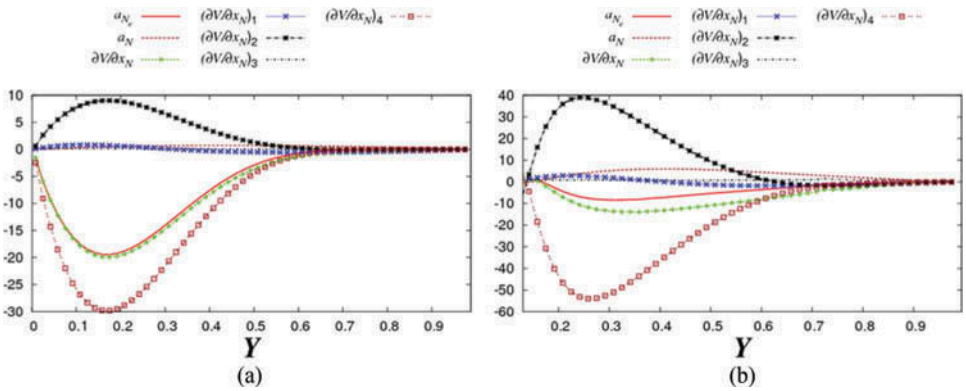

Figure 6. Average flow, a_N, 'added', $\partial V/\partial x_N$, and 'effective', a_N^e, normal strain rates conditional upon the value of Y for (a) statistically planar turbulent premixed flame and (b) turbulent jet premixed flame in a coflow. Variables are normalized with the inverse of the characteristic chemical time, $\tau_{ch}^{-1} = S_L/\delta_L$.

normal diffusion with negligible shares of the remaining terms. For $Y > 0.55$ within the preheat zone, average added strains caused by ρD variations and curvature may also contribute to $\partial V/\partial x_N$. These differences are analyzed in what follows.

Figure 7 depicts the averages of the absolute values of the flow and the chemistry 'added' normal strain rates and the Kolmogorov strain rate, ${\tau_\eta}^{-1}$, conditional on the value of Y and normalized with the characteristic chemical time, $\tau_{ch} = \delta_L/S_L$, for the two combusting flows. $|a_N|$ and ${\tau_\eta}^{-1}$ are of the same order, both in the preheat and burning zones, for the statistically planar flame; however, for $Y < 0.15$, within the burning region of the jet flame, $|a_N|$ might become one order of magnitude greater than ${\tau_\eta}^{-1}$, which is due to the interaction of the flame with the coflow of hot products. The 'added' normal strain rate due to the chemistry, $(\partial V/\partial x_N)_4$, shows entirely different trends and values from those of $|a_N|$and τ_η^{-1}; $(\partial V/\partial x_N)_4$ is, at least, one order of magnitude greater than τ_η^{-1} in both combusting flows.

It is worth pointing out that the kinetic energy dissipation rate, $\varepsilon = 2\nu s_{ij}s_{ij} - (2/3)(s_{kk})^2$, computed and used to obtain τ_η, accounts for the effect on the flow of heat addition by the flame through the volumetric dilatation rate, as shown in Figure 8. The effect of chemical heat release on the flow strain field is indirectly included in the first term of ε, while direct influences are represented by the last term. Therefore, a_N, the first term on the right side of Eq. (20), of the order of τ_η^{-1}, accounts for the flow dilatation rate due to flame heat release, whereas the last term in that equation contains an 'added' chemical strain rate.

The mean value of the inverse of $\partial V/\partial x_N$ and its four components normalized with δ_L/S_L are plotted in Figure 9 as functions of Y for the two flames. For the statistically planar flame, $(\partial V^Y/\partial x_N)^{-1}$ is mainly determined by the chemical time, τ_{chem}, and the normal diffusion time, τ_{ND}, in both the preheat and burning zones; the time scales due to ρD variations, $\tau_{\rho D}$, and to curvature changes, τ_{curv}, are one to two orders of magnitude greater than the other two times, and only for $Y > 0.45$, within a fraction of the preheat

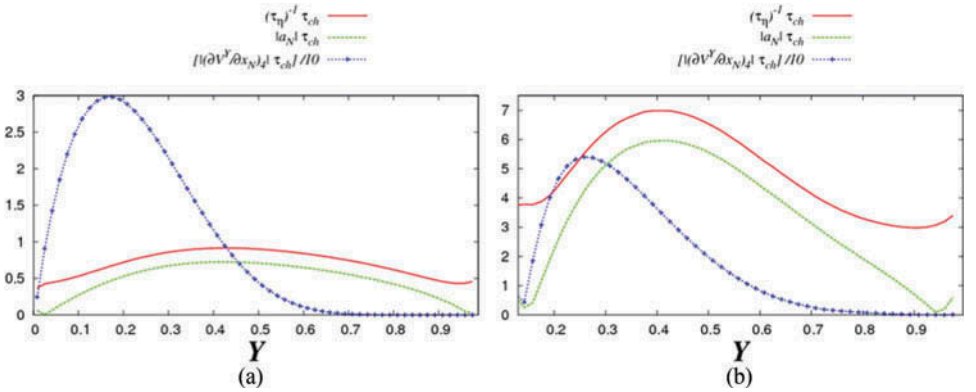

Figure 7. Average flow normal strain rate, a_N, Kolmogorov strain rate, τ_η^{-1}, and the contribution to the "added" normal strain rate due to chemical reaction, $(\partial V/\partial x_N)_4$, conditional upon Y for (a) statistically planar turbulent premixed flame and (b) turbulent jet premixed flame in a coflow. Variables are normalized with τ_{ch}. The mean value of $(\partial V/\partial x_N)_4$ is divided by 10.

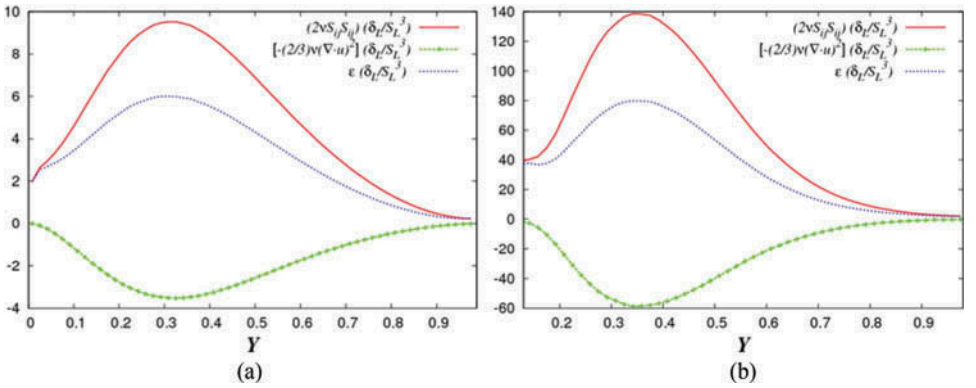

Figure 8. Average contributions to the kinetic energy dissipation rate, conditional upon Y for (a) statistically planar turbulent premixed flame and (b) turbulent jet premixed flame in a coflow. Variables are normalized with δ_L/S_L^3.

zone, $\tau_{\rho D}$, becomes relevant. The 'flow time', $|a_N|^{-1}$, is between one and two orders of magnitude greater than $(\partial V^Y/\partial x_N)^{-1}$ and the latter is the characteristic time of gradient enhancement; only for $Y > 0.45$ is the 'flow time' relevant. For the turbulent jet

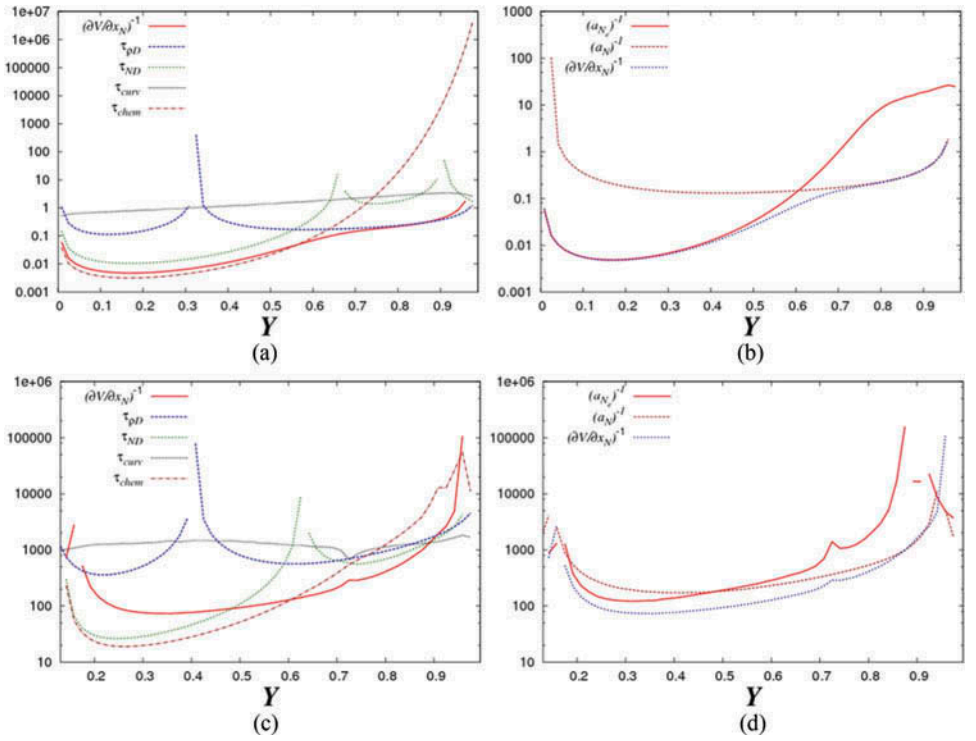

Figure 9. Terms in Eq. (20) rephrased as average characteristic times conditional upon Y for (a) and (b) statistically planar turbulent premixed flame, and (c) and (d) turbulent jet premixed flame in a coflow. Variables have been normalized with the characteristic chemical time, $\tau_{ch} = \delta_L/S_L$.

configuration, τ_{chem} and τ_{ND} are also the smallest times and, therefore, determine the value of $(\partial V^Y/\partial x_N)^{-1}$; only for $Y > 0.55$, $\tau_{\rho D}$ and τ_{curv} become comparable to τ_{ND}. However, the flow and the 'added' characteristic times are comparable within the preheat and burning zones.

Figure 10 presents the various terms on the right side of Eq. (20), redefined in terms of length variables. The length due to the normal diffusion, δ_{ND}, is at least one order of magnitude smaller than those due to ρD variations and to curvature, $\delta_{\rho D}$ and δ_{curv}, respectively, for $Y < 0.45$ (part of the preheat region and all of the burning zone plus) in the statistically planar turbulent flame (see Figure 10a); all three lengths are of the same order for $Y > 0.50$ (part of the preheat region). For the turbulent jet flame (Figure 10b), the curvature length variable is always much greater than $\delta_{\rho D}$ and δ_{ND}; the latter is about one order of magnitude smaller than the former for $Y < 0.55$ and of the same order for $Y > 0.55$.

In an attempt to make Eq. (20) dimensionless two possible cases might arise:

- Should the first term on the right side of that equation, assumed of order $\tau_{\eta 0}$, be important, the ratio of the last term, of order τ_{chem0}, to the former is:

$$\frac{\tau_{\eta 0}}{\tau_{chem0}} = \frac{\tau_{\eta 0}}{\delta_L/S_L}\frac{\delta_L/S_L}{\tau_{chem0}} = \frac{1}{Ka}\frac{1}{\frac{\tau_{chem0}}{\delta_L/S_L}} \tag{26}$$

  where δ_L and S_L are the reference laminar flame thickness and propagation speed, Ka is the Karlovitz number, and the subindex 0 denotes the characteristic magnitude of the affected variable. Similarly, the ratios of the second, third, and fourth terms to the first one are generically expressed as:

$$\frac{D_0\tau_{\eta 0}}{\delta_{\alpha 0}^2} = \frac{\tau_{\eta 0}}{\delta_L/S_L}\frac{1}{(\delta_{\alpha 0}/\delta_L)^2} = \frac{1}{Ka}\frac{1}{(\delta_{\alpha 0}/\delta_L)^2} \tag{27}$$

  where D_0 is the characteristic value of the molecular diffusion coefficient, and $\delta_{\alpha 0}$ is the characteristic magnitude of any of the three diffusive thicknesses, $\delta_{\rho D}$, δ_{ND}, and

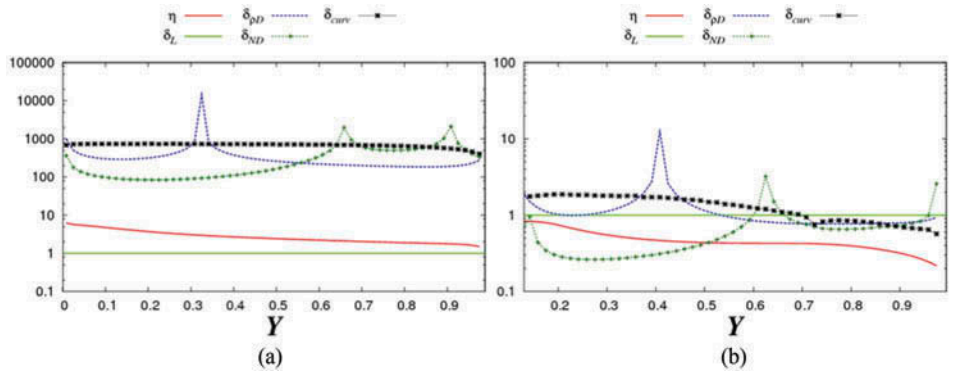

Figure 10. Terms in Eq. (20) rephrased as average length variables conditional upon Y for (a) statistically planar turbulent premixed flame and (b) turbulent jet premixed flame in a coflow. Variables are normalized with δ_L.

δ_{curv}; hence, α stands for ρD, ND, and $curv$. Both D_0 and the three $\delta_{\alpha 0}$s depend on Y and take different characteristic values in the various regions of the flames.

- On the contrary, if the last term in Eq. (20) is the dominant one, a_N would disappear from the balance, and the ratios of the second, third, and fourth terms to the last one can be written as:

$$\frac{D_0 \tau_{chem0}}{\delta_{\alpha 0}^2} = \frac{\tau_{chem0}}{\delta_L / S_L} \frac{1}{(\delta_{\alpha 0}/\delta_L)^2} \tag{28}$$

All symbols have the same meaning of the previous case. From Figures 7, 9, and 10, one can readily elaborate Tables 2 and 3 for the different ratios.

Therefore, from Table 2 for the statistically planar flame, it is apparent that for $Y < 0.5$, the chemical term, the last one on the right side of Eq. (20), will determine the time rate of change of Δx_N, and, therefore, of the scalar gradients. For $0.5 < Y < 0.7$, within the preheat zone, the flow normal strain rate and the chemical term become comparable. On the contrary, a_N and τ_{chem}^{-1} are of the same order, both in the preheat and the burning regions of the turbulent jet flame; for $Y < 0.5$ the normal diffusion term contributes to change Δx_N, whereas effects due to ρD spatial variations and curvature are negligible. All terms contribute to the balance in different degrees for $Y > 0.5$.

Some authors (Hartung et al., 2008) proposed to estimate the mean thickness of a turbulent flame using:

$$\delta_{1/|\nabla Y|} = \frac{1}{|\nabla Y|} \tag{29}$$

An alternative definition is possible, realizing that the local and instantaneous 'surface density function', defined by (Pope, 1988; Vervisch et al., 1995):

$$\Sigma(\Gamma; \mathbf{x}, t) = |\nabla Y| \delta[\Gamma - Y(\mathbf{x}, t)] \tag{30}$$

Table 2. Dimensionless ratios for the statistically planar turbulent premixed flame.

Y	0.05	0.10	0.20	0.30	0.40	0.50	0.60	0.70	0.80	0.90	0.95
$\tau_{chem0}/(\delta_L/S_L)$	0.061	0.038	0.034	0.046	0.085	0.225	0.930	7.65	194.24	40,127	2.561×10^6
$\tau_{\eta 0}/(\delta_L/S_L)$	2.20	1.88	1.39	1.16	1.09	1.11	1.18	1.33	1.61	2.13	2.31
$\delta_{\rho D0}/\delta_L$	371.81	301.32	316.81	675.47	378.83	258.87	219.85	199.73	187.11	189.46	219.03
δ_{ND0}/δ_L	128.89	98.07	84.54	89.90	111.26	165.23	349.45	627.00	507.97	1485.21	460.73
δ_{curv0}/δ_L	734.78	741.35	746.03	736.81	732.56	719.85	708.15	682.58	646.32	567.63	481.77

Table 3. Dimensionless ratios for the turbulent jet premixed flame in a coflow.

Y	0.05	0.10	0.20	0.30	0.40	0.50	0.60	0.70	0.80	0.90	0.95
$\tau_{chem0}/(\delta_L/S_L)$	1.72	0.08	0.023	0.019	0.027	0.050	0.12	0.37	1.21	9.01	36.6
$\tau_{\eta 0}/(\delta_L/S_L)$	0.40	0.31	0.23	0.15	0.14	0.15	0.18	0.24	0.30	0.33	0.31
$\delta_{\rho D0}/\delta_L$	19.40	5.27	1.02	1.12	5.88	1.15	0.84	0.77	0.77	0.79	0.84
δ_{ND0}/δ_L	4.14	0.48	0.29	0.26	0.30	0.42	1.02	0.77	0.65	0.74	0.90
δ_{curv0}/δ_L	2.14	1.62	1.82	1.80	1.72	1.52	1.24	0.98	0.84	0.70	0.65

is apparently expressible as:

$$\Sigma(\Gamma;\mathbf{x},t)=\frac{1}{\Delta x_N(\Gamma;\mathbf{x},t)} \tag{31}$$

Thus, the relationship:

$$\frac{1}{|\nabla Y|_{Y(x,t)=\Gamma}}=\Delta x_N(\Gamma;\mathbf{x},t)\delta[\Gamma-Y(\mathbf{x},t)] \tag{32}$$

holds. The average of the two sides yields:

$$\left\langle\frac{1}{\langle\nabla Y\rangle}|Y(\mathbf{x},t)=\Gamma\right\rangle=\langle\Delta x_N|Y(\mathbf{x},t)=\Gamma\rangle P_Y(\Gamma;\mathbf{x},t) \tag{33}$$

where $P_Y(\Gamma;\mathbf{x},t)$ is the PDF of $Y(\mathbf{x},t)$.

Therefore,

$$\langle\Delta x_N|Y(\mathbf{x},t)=\Gamma\rangle=\frac{1}{P_Y(\Gamma;\mathbf{x},t)}\left\langle\frac{1}{\langle\nabla Y\rangle}|Y(\mathbf{x},t)=\Gamma\right\rangle. \tag{34}$$

$\langle\Delta x_N|Y(\mathbf{x},t)=\Gamma\rangle$ seems a consistent alternative definition for the mean thickness of the turbulent flame.

Figure 11 depicts the average values of $\delta_{1/|\nabla Y|}$ and $\langle\Delta x_N|Y(\mathbf{x},t)=\Gamma\rangle$, conditional upon Y for the two flames. Our definition provides turbulent flame thicknesses, which are approximately constant over all values of Y. The previous definition (Sankaran, 2007) yields values between 5 and 10 times the laminar flame thickness, while ours are slightly higher and around 15 for the statistically planar flame. On the other hand, our estimation of the average turbulent jet flame thickness is about 15 times that of the laminar flame, compared to a value between 1 and 2 using the previous definition. No regions of Y where the laminar flame thickness is greater than the turbulent one are encountered with either definition for the two flames. The red lines in Figure 11 are estimates for Δx_N, obtained using the values of Y and $|\nabla Y|$ through interpolation in a cubic box containing 27 grid points.

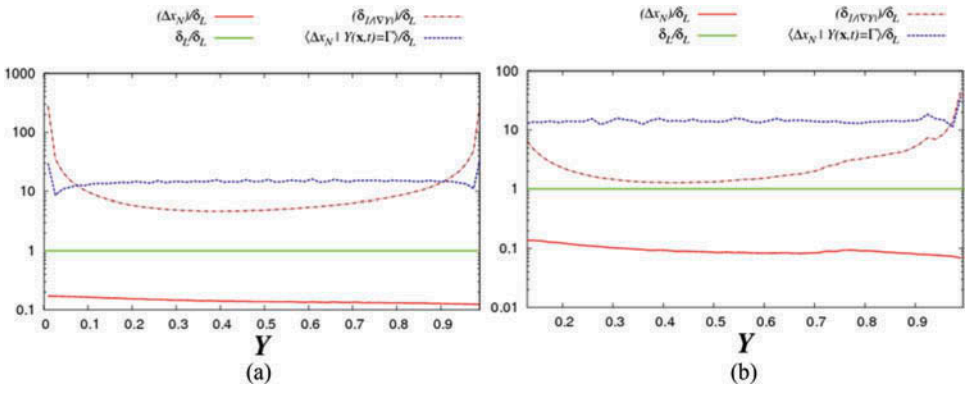

Figure 11. Average thicknesses, $\delta_{1/|\nabla Y|}$ and $\langle\Delta x_N|Y(\mathbf{x},t)=\Gamma\rangle$, conditional upon Y for (a) statistically planar turbulent premixed flame and (b) turbulent jet premixed flame in a coflow. Variables are normalized with δ_L.

5. Some modeling considerations

Swaminathan and Bray (2011) have summarized different approaches to model turbulent transport and chemical conversion for both RANS and LES formulations. In this section, the closure of the molecular mixing term in the scalar PDF transport equation is scrutinized. The molecular diffusion contribution to the conservation equation for Y is given by the first three terms on the right side of Eq. (7), which, averaged and conditioned on the scalar value, yield the molecular mixing term in the scalar PDF methodology. Figure 12 shows the average of the molecular diffusion term and these three contributions are conditional upon the value of Y for the two flames. Although the normal diffusion is the most important share, those due to ρD variations and to tangential diffusion (curvature) are by no means negligible in some ranges of scalar values.

In this section, attention is focused on the modeling of the classical normal diffusion, $D\left(\partial^2 Y/\partial x_N^2\right)$. This term can be discretized using central finite differences as:

$$D\frac{\partial^2 Y}{\partial x_N^2} = \frac{D}{(\Delta x_N)^2}\left[Y(x_N + \Delta x_N) - 2Y(x_N) + Y(x_N - \Delta x_N)\right] \tag{35}$$

with

$$Y(x_N + \Delta x_N) \geq 2Y(x_N) \geq Y(x_N - \Delta x_N) \tag{36}$$

An unknown characteristic mixing time, $\tau_M = (\Delta x_N)^2/D$, appears naturally; the choice of this time is discussed in what follows. A Monte Carlo simulation of this expression would require sorting out particles fulfilling the restriction (36). The implications of this model are currently under evaluation.

On the other hand, the normal diffusion term can also be expressed as:

$$D\frac{\partial^2 Y}{\partial x_N^2} = -\frac{6D}{(\Delta x_N)^2}\left[Y(x_N, t) - Y(x_N, t)_{2\Delta x_N}\right] \tag{37}$$

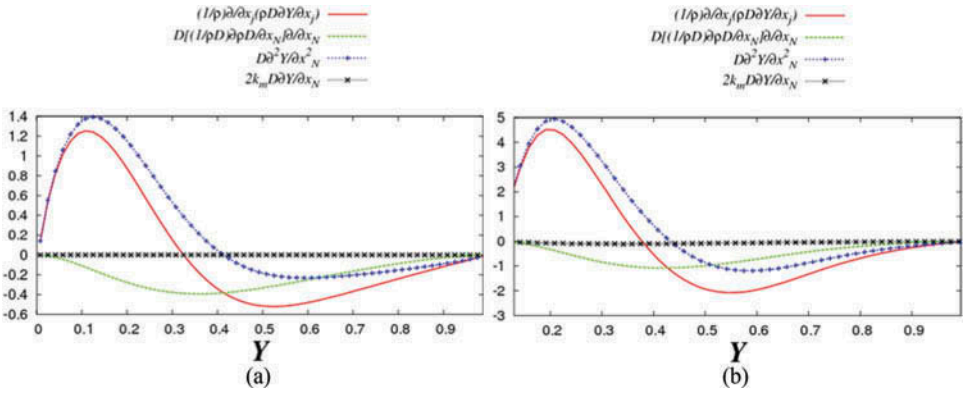

Figure 12. Average molecular diffusion term and its three contributions [Eq. (7)] conditional upon Y for (a) statistically planar turbulent premixed flame and (b) turbulent jet premixed flame in a coflow. Variables have been normalized with the characteristic chemical time, $\tau_{ch} = \delta_L/S_L$.

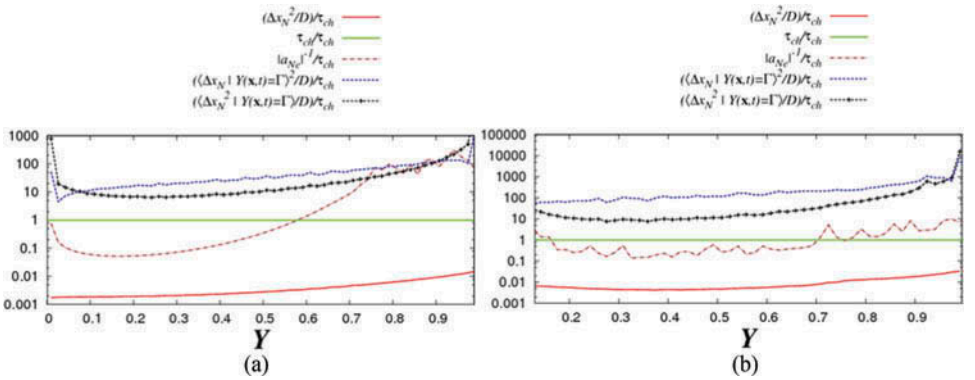

Figure 13. Possible characteristic mixing times as functions of Y for (a) statistically planar turbulent premixed flame and (b) turbulent jet premixed flame in a coflow. Variables are normalized with τ_{ch}.

where the local average on the right side is given by:

$$\langle Y(x_N,t)\rangle_{2\Delta x_N} = \frac{1}{2\Delta x_N}\int_{x_N-\Delta x_N}^{x_N+\Delta x_N} Y(x_N,t)dx_N \tag{38}$$

This is an excellent approximation for the normal diffusion if Δx_N is much smaller than the length microscales over which $Y(\mathbf{x},t)$ fluctuates, namely, for a DNS of the scalar field. The mixing time, $\tau_M = (\Delta x_N)^2/D$, appears again in this closure. The previous expression [Eq. (37)] resembles the linear mean square estimation (LMSE) closure (Dopazo and O'Brien, 1974) with the global scalar mean replaced by the local average. The implementation of the previous closure assumption using a local mean improves results for the inert scalar mixing of an initially binary field in constant density turbulence and is currently under scrutiny.

The choice of the mixing time is a critical issue. Two physically sound characteristic times, which directly determine the scalar gradient evolution, might be either $\langle \Delta x_N | Y(\mathbf{x},t)=\Gamma\rangle^2/D$ or $\langle (\Delta x_N)^2 | Y(\mathbf{x},t)=\Gamma\rangle/D$. These two choices are shown in Figure 13, and are compared with the effective characteristic normal strain time, $\left(\left|a_N^e\right|\right)^{-1}$. The latter and $\langle (\Delta x_N)^2 | Y(\mathbf{x},t)=\Gamma\rangle/D$ display similar trends, although $\left(\left|a_N^e\right|\right)^{-1}$ is between one and two orders of magnitude smaller than the proposed mixing time. The red lines in Figure 13 correspond to time scales estimated using Δx_N in Figure 11.

6. Conclusions

Equations for the absolute value of the scalar gradient and for the infinitesimal distance between two iso-scalar non-material surfaces have been obtained. Both equations show that the 'effective' strain rate normal to the iso-surfaces is an essential variable determining the enhancement or destruction of scalar gradients and the reduction or growth of the infinitesimal distance between non-material surfaces. That 'effective' normal strain rate is the addition of the flow normal strain rate plus an 'added' contribution, which includes molecular diffusion and chemical conversion. The 'added' normal strain rate is generated

by variations of the iso-surface propagation speeds normal to them and can be comparable to smaller or greater than the flow normal strain rate.

Two DNS datasets for turbulent premixed flames have been examined: the first simulates a statistically planar propagating front in an inflow-outflow configuration, while the second computes a jet injecting a methane-air mixture surrounded by a coflow of hot products. In both combusting cases the flow normal strain rates are predominantly positive, whereas the 'added' normal strain rate is negative, with a magnitude greater than the former. Thus, scalar gradients tend to be enhanced. This explains previous results in the literature (Chakraborty and Swaminathan, 2007; Chakraborty et al., 2009; Swaminathan and Grout, 2006).

Use of dimensionless time $[t/(\delta_L/S_L)]$ and infinitesimal distance $(\Delta x_N/\delta_L)$, leads to an equation (20) for the time rate of change of the distance between two adjacent iso-surfaces, which depends on the dimensionless parameters $\left[(\delta_L/S_L)/\tau_{\eta 0}\right]$, $(\delta_{\delta D_0}/\delta_L)$, (δ_{ND_0}/δ_L), $(\delta_{curv0}/\delta_L)$, and $[\tau_{chem0}/(\delta_L/S_L)]$. The first is the Karlovitz number. For the two flames examined, flow normal strain rate is shown to accurately scale with the inverse of the Kolmogorov time microscale, which includes the effects of volumetric dilatation caused by the chemical heat release. When $Ka[\tau_{chem0}/(\delta_L/S_L)] \ll 1$, the flow normal strain rate is much smaller that the chemical added normal strain rate; this is apparently the case for the burning and part of the preheat regions of the statistically planar flame. On the other hand, if $Ka[\tau_{chem0}/(\delta_L/S_L)]\sim 1$ the effects of the flow and added normal strain rates are comparable; this occurs in the turbulent jet premixed flame. The values of the various dimensionless groups depend of the flame and on the region considered. Large values of $(\delta_{\delta D_0}/\delta_L)$, (δ_{ND_0}/δ_L), and $(\delta_{curv0}/\delta_L)$, shown in Tables 2 and 3, likely provide hints of a Reynolds and/or Damköhler number dependence that must be investigated. Relevant terms in the balance equation in different regions of the computational domain in terms of the reduced mass fraction have been scrutinized.

A new and consistent definition for the mean thickness of a turbulent premixed flame based on the equivalence of the surface density function and the inverse of the length between two adjacent iso-scalar surfaces has been proposed and computed from the examined DNS data and compared to a previous proposal (Sankaran et al., 2007).

Finally, some modeling considerations for the molecular mixing term entering scalar PDF transport equations have been presented. Two approaches have been suggested: one uses the finite difference approximation for second derivatives, whereas the other is equivalent to a LMSE with the local mean. In both approximations a characteristic mixing time appears naturally, which is conjectured to be proportional to the inverse of the 'effective' normal strain rate. Preliminary calculations show one to two orders of magnitude differences. Alternative molecular mixing times are currently being tested.

Acknowledgments

The authors are indebted to Dr. Carmen Jimenez and Professors Luc Vervisch and Pascale Domingo for kindly allowing them to use their DNS datasets and for providing useful criticism and suggestions. This manuscript has not been submitted or published elsewhere. The results presented and discussed in the manuscript are originals. No data have been fabricated or manipulated to support the conclusions. No data, text, or theories by others are presented as if they were the authors' own.

Funding

Luis Cifuentes gratefully acknowledges the economic support of the Spanish Ministry of Economy and Competitiveness, under the CONSOLIDER-INGENIO Program, Project CS D2010-00011-SCORE, which C.D. coordinates.

ORCID

Luis Cifuentes http://orcid.org/0000-0001-9077-2597

References

Aris, R. 1962. *Vectors, Tensors and the Basic Equations of Fluid Mechanics*, Prentice-Hall, Inc., Englewood Cliffs, NJ.

Ashurst, W., Kerstein, A., Kerr, R., and Gibson, C. 1987. Alignment of vorticity and scalar gradient in simulated Navier-Stokes turbulence. *Phys. Fluids*, **30**(8), 2343–2353.

Borghi, R. 1985. On the structure and morphology of turbulent premixed flames. In C. Bruno and C. Casci (Eds.), *Recent Advances in Aerospace Science*, Plenum Press, New York, pp. 117–138.

Celis, C., and Da Silva, L.F.F. 2015. Lagrangian mixing models for turbulent combustion: Review and prospects. *Flow Turbul. Combust.*, **94**(3), 643–689.

Chakraborty, N. 2007. Comparison of displacement speed statistics of turbulent premixed flames in the regimes representing combustion in corrugated flamelets and thin reaction zones. *Phys. Fluids*, **19**(10), 105109.

Chakraborty, N., and Cant, S. 2004. Unsteady effects of strain rate and curvature on turbulent premixed flames in inlet-outlet configuration. *Combust. Flame*, **137**(1), 129–147.

Chakraborty, N., and Cant, S. 2005. Influence of Lewis number on curvature effects in turbulent premixed flame propagation in the thin reaction zones regime. *Phys. Fluids*, **17**(10), 105105.

Chakraborty, N., Klein, M., and Swaminathan, N. 2009. Effects of Lewis number on the reactive scalar gradient alignment with local strain rate in turbulent premixed flames. *Proc. Combust. Inst.*, **32**, 1409–1417.

Chakraborty, N., and Swaminathan, N. 2007. Influence of the Damköhler number on turbulence-scalar interaction in premixed flames. I. Physical insight. *Phys. Fluids*, **19**(4), 045103.

Cifuentes, L. 2015. Local flow topologies and scalar structures in turbulent combustion, Ph.D. Dissertation, University of Zaragoza, Zaragoza, Spain.

Cifuentes, L., Dopazo, C., Martin, J., Domingo, P., and Vervisch, L. 2014. Local volumetric dilatation rate and scalar geometries in a premixed methane-air turbulent jet flame. *Proc. Combust. Inst.*, **35**, 1295–1303.

Cifuentes, L., Dopazo, C., Martin, J., Domingo, P., and Vervisch, L. 2016. Effect of the local flow topologies upon the structure of a premixed methane-air turbulent jet flame. *Flow Turbul. Combust.*, **96**(2), 535–546.

Cuenot, B., Bedat, B., and Corjon, A. 1997. NTMIX3D User's Guide, volume 1.0. CERFACS, CFD - COMBUSTION. http://cerfacs.fr/logiciels-de-simulation-pour-la-mecanique-des-fluides.

Dopazo, C. 1994. Recent developments in pdf methods. In P. Libby and F.A. Williams (Eds.), *Turbulent Reactive Flows*, Academic Press, New York.

Dopazo, C., and O'Brien, E.E. 1974. An approach to the auto-ignition of a turbulent mixture. *Acta Astronaut.*, **1**, 1239–1266.

Dopazo, C., Cifuentes, L., Hierro, J., and Martin, J. 2015b. Micro-scale mixing in turbulent constant density reacting flows and premixed combustion. *Flow Turbul. Combust.*, **96**(2), 547–571.

Dopazo, C., Cifuentes, L., Martin, J., and Jimenez, C. 2015a. Strain rates normal to approaching iso-scalar surfaces in a turbulent premixed flame. *Combust. Flame*, **162**, 1729–1736.

Echekki, T., and Chen, J.H. 1999. Analysis of the contributions of curvature to premixed flame propagation. *Combust. Flame*, **118**, 308–311.

Flagan, R.C., and Appleton, J.P. 1974. A stochastic model of turbulent mixing with chemical reaction: Nitric oxide formation in a plug-flow burner. *Combust. Flame*, **23**, 249–267.

Hartung, G., Hult, J., Kaminski, C.F., Rogerson, J.W., and Swaminathan, N. 2008. Effect of heat release on turbulence and scalar-turbulence interaction in premixed combustion. *Phys. Fluids*, **20**(3), 035110.

Haworth, D.C. 2010. Progress in probability density function methods for turbulent reacting flows. *Prog. Energy Combust. Sci.*, **36**, 168–259.

Masri, A.R. 2015. Partial premixing and stratification in turbulent flames. *Proc. Combust. Inst.*, **35**, 1115–1136.

O'Brien, E.E. 1980. The probability density function (pdf) approach to reacting turbulent flows. In P. Libby and F.A. Williams (Eds.), *Turbulent Reacting Flows*, Springer-Verlag, Berlin, pp. 185–218.

Orszag, S., and Patterson, G. 1972. Numerical simulation of three-dimensional homogeneous isotropic turbulence. *Phys. Rev. Lett.*, **12**, 76–79.

Poinsot, T., and Lele, S.S. 1992. Boundary conditions for direct simulations of compressible viscous flows. *J. Comput. Phys.*, **101**, 104–129.

Poinsot, T., and Veynante, D. 2005. *Theoretical and Numerical Combustion*, R. T. Edwards, Inc., Philadelphia.

Pope, S.B. 1985. Pdf methods for turbulent flows. *Prog. Energy Combust. Sci.*, **11**, 119–192.

Pope, S.B. 1988. The evolution of surfaces in turbulence. *Int. J. Eng. Sci.*, **26**, 445–469.

Sankaran, R., Hawkes, E.R., Chen, J.H., Lu T., and Law, C.K. 2007. Structure of a spatially developing turbulent lean methane-air Bunsen flame. *Proc. Combust. Inst.*, **31**, 1291–1298.

Steinberg, A.M., Driscoll, J.F., and Swaminathan, N. 2012. Statistics and dynamics of turbulence-flame alignment in premixed combustion. *Combust. Flame*, **159**, 2576–2588.

Swaminathan, N., and Bray, K.N.C. (Eds.). 2011. *Turbulent Premixed Flames*, Cambridge University Press, Cambridge, UK.

Swaminathan, N., and Grout, R.W. 2006. Interaction of turbulence and scalar fields in premixed flames. *Phys. Fluids*, **18**(4), 045102.

Vervisch, L., Bidaux, E., Bray, K.N.C., and Kollmann, W. 1995. Surface density function in premixed turbulent combustion modeling. Similarities between probability density function and flame surface approaches. *Phys. Fluids*, **7**, 2496–2503.

Yeung, P.K., Girimaji, S.S., and Pope, S.B. 1990. Straining and scalar dissipation on material surfaces in turbulence: Implications for flamelets. *Combust. Flame*, **79**, 340–365.